Short Communication

**Nanomedicine**

# Hydrodenticity to enhance relaxivity of gadolinium-DTPA within crosslinked hyaluronic acid nanoparticles

**Aim:** The efficacy of gadolinium (Gd) chelates as contrast agents for magnetic resonance imaging remains limited owing to poor relaxivity and toxic effects. Here, the effect of the hydration of the hydrogel structure on the relaxometric properties of Gd-DTPA is explained for the first time and called *Hydrodenticity*. **Results:** The ability to tune the hydrogel structure is proved through a microfluidic flow-focusing approach able to produce crosslinked hyaluronic acid nanoparticles, analyzed regarding the crosslink density and mesh size, and connected to the characteristic correlation times of the Gd-DTPA. **Conclusion:** *Hydrodenticity* explains the boosting (12-times) of the Gd-DTPA relaxivity by tuning hydrogel structural parameters, potentially enabling the reduction of the administration dosage as approved for clinical use.

Maria Russo‡,1,2, Alfonso Maria Ponsiglione‡,1,2, Ernesto Forte3, Paolo Antonio Netti1,2,4 & Enza Torino*,2,4

1Department of Chemical, Materials & Production Engineering, University of Naples Federico II, Piazzale V. Tecchio 80, 80125 Naples, Italy
2Center for Advanced Biomaterials for Healthcare IIT@CRIB, Istituto Italiano di Tecnologia (IIT), Largo Barsanti e Matteucci 53, 80125 Naples, Italy
3IRCCS SDN, Via E. Gianturco 113, 80143 Naples, Italy
4Interdisciplinary Research Center on Biomaterials, University of Naples Federico II, Piazzale V. Tecchio 80, 80125 Naples, Italy
*Author for correspondence:
Tel.: +3908119933100
enza.torino@iit.it
‡Authors contributed equally

**Hydrodenticity to enhance relaxivity of Gd-DTPA within crosslinked hylaluronic acid nanoparticles (cHANPs)**
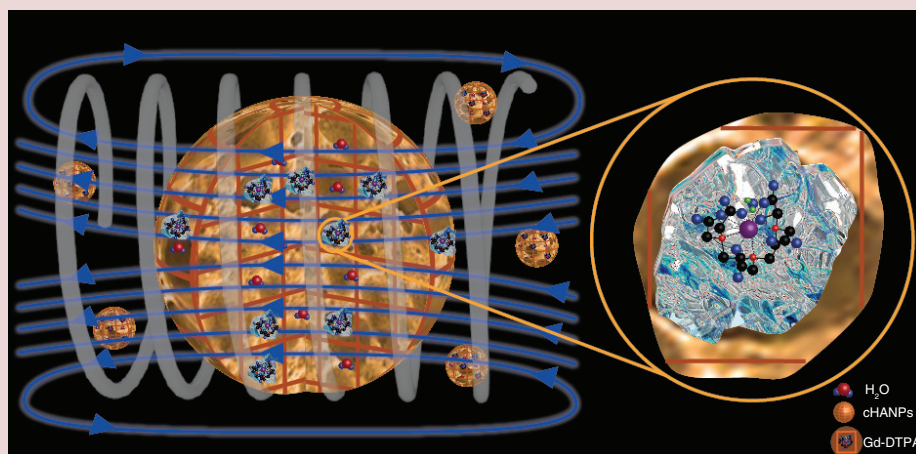
H₂O
cHANPs
Gd-DTPA

During the past 30 years, magnetic resonance imaging (MRI) has emerged as an established technique for preclinical imaging and clinical diagnosis [1–4]. Although MRI enables visualization of tissues at high spatial resolution without using ionizing radiation

Future Medicine part of fsg

or invasive procedures, its sensitivity is significantly lower than other imaging modalities, such as PET/single-photon emission computed tomography [5–8]. Performances of MRI examinations can be improved by using contrast agents (CAs), which allow the differentiation of tissues that would otherwise be indistinct [9–11].

The presence of the CA causes a significant increase in the relaxation rate of the water proton nearby paramagnetic ions, thereby adding details to the anatomical resolution. Thanks to its very high magnetic moment, gadolinium (Gd) is the most frequently used metal ion for MRI. However, owing to the toxicity of free Gd ions [6], which can induce nephrogenic system fibrosis, Gd-chelates, such as Gd-DTPA (Magnevist, Schering AG) [12], are commonly used in contrast-enhanced examinations [5,13].

Currently, more than 35% of all clinical MRI scans utilize the injection of clinically approved Gd-based CAs (GdCAs) intravenously [5]. Despite this widespread use, some concerns arise from CAs' efficacy, mainly limited by their concentration (mM) and relaxivity ($r_1$, mM$^{-1}$s$^{-1}$). Other concerns are related to low tissue specificity, nephrotoxicity, long scan time and rapid renal clearance, which significantly reduce the time window for clinical imaging acquisitions [14,15]. Furthermore, McDonald *et al.* [16] have recently reported results about intracranial Gd deposition after repeated intravenous administration of CAs even if these signal intensity changes are not specific and can be seen with several other pathologic conditions.

The poor relaxivity of commercial CAs, much below its theoretically maximal value [17,18], has led to the development of novel macromolecules conjugating CAs [1,19–24]. As stated by Solomon–Bloembergen–Morgan theory [25,26], indeed, high relaxivity can be achieved by controlling the characteristic parameters that regulate the dipolar interaction between water protons and GdCAs [5]. The main characteristic parameters include: the number of water molecules (q) in the inner sphere, in other words, those present in the coordination sites of the Gd ion and their residence lifetime ($T_M$); the rotational correlation time of the metal complex ($T_R$); the diffusion correlation time ($T_D$) of the water molecules in the outer sphere, in other words, those diffusing nearby the metal complex.

These parameters can be tuned by exploiting the versatile properties of nano- and bio-materials and a wide range of nanostructured CAs with enhanced relaxivity can be developed [17,27–33]. We have recently published some works in this field explaining the impact of biopolymer matrices on relaxometric properties of CAs [34] and showing a microfluidic approach to produce hydrogel nanoparticles loading clinically relevant GdCAs, improving relaxometric properties of CAs without their chemical modification [35]. Other authors also proposed some strategies to fabricate nanostructures based on the effect of rigidification [36] and confinement [37] of metal-chelates [38] to boost relaxometric properties [39].

Despite the valuable role of the CAs for MRI, this case history confirms the importance of developing systems able to enhance relaxivity of clinical relevant GdCAs and also to protect the chelate from transmetallation phenomena and control accumulation and clearance in a specific organ [40–42].

In this scenario, we have proved that, by changing structural parameters of an hydrogel matrix containing a CA through a microfluidic flow-focusing (MFF) approach, it is possible to affect the dipolar coupling between the electronic magnetic moment of the metal ion and the nuclear magnetic moment of the water protons (relaxation rate). This effect results from the complex equilibrium established by the elastic stretches of polymer chains, water osmotic pressure and hydration degree of GdCAs, that we have called *Hydrodenticity*.

*Hydrodenticity*, hence, refers to the status of the hydrated Gd-DTPA with the coordination water subjected to osmotic pressure [43] deriving from elastodynamics equilibrium of swollen gels [44–46]. We hypothesize that the attainment of this equilibrium is reached when the normal energetic stability of the meshes is compromised by the presence of the Gd-DTPA and evolves to a new spontaneous equilibrium involving the formation of nanocompartments, here called 'Gado-Meshes', in which water is in an abnormal aggregate state that influences the relaxivity. The capability to control the organization of these nanocompartments within the nanoparticles can be applied to define a new class of medical products useful to improve the properties of CAs for MRI.

The tunability of the hydrogel properties is here achieved by a microfluidic adjustable and high-throughput strategy, already proposed to produce intravascularly-injectable and biocompatible Gd-DTPA-loaded crosslinked hyaluronic acid nanoparticles (cHANPS) for MRI [35]. Within the cHANPs, the properties of *Hydrodenticity* can be modulated to obtain desired crosslink density, mesh size, hydrophilicity and loading capability, playing on the biodegradable behavior and relaxometric properties of the Gd-loaded cHANPs. Indeed, nanoparticles with a mean particle size as low as 35 nm are obtained without the chemical modification of the clinically approved chelate, achieving a signal intensity in $r_1$ 12-times larger than that of the commercial MRI CA, Magnevist, at the magnetic field used in clinical MRI, 1.5 Tesla.

## Materials & methods
### Materials
Sodium hyaluronate (Mw = 42 kDa) is purchased from Bohus Biotech (Sweden). Diethylenetri-aminepentaacetic acid gadolinium(III) dihydrogen salt hydrate Gd-DTPA (empirical formula: $C_{14}H_2OGdN_3O_{10} \times H_2O$; Mw = 547.57 g/mol). Nonionic surfactant Span80 (formula $C_{24}H_{44}O_6$ formula weight: 428.62 g/mol). Divinyl sulfone (or vinyl sulfone) (DVS) contains <650 p.p.m. hydroquinone as inhibitor (purity 97%; density 1.117 g/ml at 25°C (lit.); molecular formula: $C_4H_6O_2S$; Mw = 118.15 g/mol). Acetone (CHROMASOLV, for HPLC ≥99.8; molecular formula: $CH_3COCH_3$; Mw = 58.08 g/mol). Ethanol (ACS reagent, ≥99.5 [200 proof], absolute; molecular formula: $CH_3CH_2OH$; Mw = 46.07 g/mol). Sodium hydroxide NaOH (ACS reagent, ≥97.0%, Mw = 40.00 g/mol). Gadolinium chloride solution $GdCl_3$ (Mw = 263.61 g/mol) and sodium chloride NaCl (ACS reagent, ≥99.0%, Mw = 58.44 g/mol) are purchased from Sigma-Aldrich Co. The water, used for synthesis and characterization, is purified by distillation, deionization and reserve osmosis (Milli-Q Plus).

### Microfluidic set-up for flow-focusing approach
Our microfluidic device 'Droplet Junction Chip' (depth × width 190 μm × 390 μm) is purchased from Dolomite Centre Ltd. It is a glass microfluidic device designed for generating droplets. The internal surface of the channel is coated with the hydrophobic material. On the chip there are two separate droplet junctions (see Supplementary Figure 1), which can be used in combination. For our experiments, we used only X-junction with three inlet channels and a single outlet channel that can be used to mix and react three reagents. The device has a flow-focusing geometry with 90° angle between the inlets to enhance the diffusion process. It is compatible with Chip interface H for fluidic connections. Three-way isolation ethylene tetrafluoroethylene valves, connected to the syringes and the microfluidic device, make the automatic fill-in of the syringes feasible, thus allowing a continuous dispensing of reagents. The linkage between fluorinated ethylene propylene tubes and device is carried out through a specially designed connection with polytetrafluoroethylene connectors. The flow focusing behavior on the microchannel is observed using an optical fluorescence microscope (Olympus IX71) with a 4× scanning objective.

### Microfluidic route of production & characterization
Multiple factors influencing the production process of cHANPs through the microfluidic platform have been evaluated in a previous publication [35]. Main steps of this protocol and furthers used in the present work are summarized here:

- Flow rate ratio: ratio between the solvent volumetric flow rate and the nonsolvent volumetric flow rate (see paragraph "Preparation of nanoparticles" and Supplementary Information);

- Crosslinking strategy: premix of divinyl sulfone into the middle channel or adding DVS into the side channels (see paragraph "Crosslinking reaction by DVS" and Supplementary Information);

- Effect of crosslinking agent's concentration, process temperature, type of surfactant, NaOH and NaCl concentration and other parameters have been widely discussed in our previous work [35].

After the nanoparticles' synthesis, further properties of cHANPs are also evaluated:

- Loading capability (see paragraph "Loading capability" and Supplementary Information);

- Stability in water (see paragraph "Stability and release study of cHANPs" and Supplementary Information);

- Longitudinal relaxation times, rates and relaxivity (see paragraph "*In vitro* relaxivity study" and Supplementary Information);

- Swelling ratio (SR) (see paragraph "Swelling ratio and hydrogel parameters" and Supplementary Information).

Finally, the following hydrogel structural parameters are theoretically computed and their relationships with relaxation parameters are evaluated:

- Crosslink density (see paragraph "Swelling ratio and hydrogel parameters" and Supplementary Information);

- Mesh size (see paragraph "Swelling ratio and hydrogel parameters" and Supplementary Information).

### Preparation of nanoparticles
Different flow rates are tested and the influence of the flow rate ratio is determined. For the feasibility study, a 5 ml aqueous solution containing hyaluronic acid (HA), concentrations ranging from 0.01 to 0.1% w/v, is used to examine the effect of the nanoprecipitation by flow focusing only due to the concentration of the polymer. Higher HA concentrations provide massive precipitation, causing a strong interference on the flow focusing and consequently on the nanoparticle

size. Among several tested molecular weights of HA, 42 kDa is selected as the optimal one because it can provide smaller nanoparticles. The initial solution is kept under continuous stirring for at least 4 h and then injected through the middle channel. The middle flow rate is ranged from 5 to 100 μl/min. A nonsolvent, in other words, acetone as suggested elsewhere [47], is injected through the side channels to induce nano-precipitation by a flow-focusing approach. Side flow rates are changed from 50 to 300 μl/min, with a step of 10 μl/min. Precipitated nanoparticles are collected in a Petri glass containing few milliliters of nonsolvent and kept under continuous stirring. The stirring, conducted over 8 h, is used to promote the diffusion of DVS and consequently to improve the crosslinking reaction. Each experiment is repeated many times.

### Crosslinking reaction by DVS

Crosslinking reaction by DVS is studied in the microfluidic system at a concentration of NaOH and NaCl ranging from 0.1 to 0.3 M and from 0.02 to 0.2 M, respectively. Acetone, ethanol and isopropanol are tested as nonsolvent and are introduced in the side micro-channels, as already explained in our previous work [35].

Two crosslinking scenarios are investigated: premix of DVS into the middle channel or adding DVS into the side channels. The crosslinking agent is injected, alternatively, into the side channels or in the middle channel at different concentrations, ranging from 0 to 8% v/v and from 0 to 20% v/v, respectively.

Three different surfactants are tested at various reagent concentrations and flow rates. Tween-85 (ranging from 0.5 to 1% w/v), Tween-21 (ranging from 0.5 to 3% w/v) and Span 80 (ranging from 0.5 to 1.5% w/v), are mixed to the nonsolvent or to the aqueous solution. In the first scenario, the solvent phase also containing DVS is kept at a constant T of 5°C to avoid undesired crosslinking effects; the device is instead heated to 35°C.

### Purification, recovery and characterization of nanoparticles

Purification is performed by a solvent gradient dialysis or by ultracentrifugation. Typically, 2 ml of the produced nanoparticles are collected and used for further analysis and size characterization. A Spectra Por Cellulose Membrane 6 (Molecular Weight Cut Off MWCO 50,000) is used for purification protocol. A typical procedure consists of loading collected samples into dialysis tube and keeping the buffer solution (phosphate-buffered saline [PBS], pH 6.8, room temperature; final concentration of 10 mM $PO_4^{3-}$, 137 mM NaCl and 2.7 mM KCl) under continuous stirring at 130 r.p.m.

to increase the diffusion rate. The first purification step is in ethanol:

- Purify the sample for 2 h in 70% Acetone + 30% Ethanol; 2 h in 50% Acetone + 50% Ethanol; 2 h in 30% Acetone + 70% Ethanol; 2 h in 100% Ethanol.

The second purification step is in water:

- Purify the sample for 2 h in 70% Ethanol + 30% MilliQ water; 2 h in 50% Ethanol + 50% MilliQ water; 2 h in 30% Ethanol + 70% MilliQ water; 2 h in 100% MilliQ water.

The concentration gradient of water is slowly added to the buffer solution to avoid aggregation and diffusion phenomena across the membrane. Dynamic light scattering is used to determine nanoparticle size. Nanoparticles are concentrated by ultracentrifugation. The recovery is performed at 15°C, at 80,000 r.p.m. for 15 min. After these treatments, a 100 μl of purified samples are deposited on a polycarbonate Isopore membrane filter (0.05, 0.1 and 0.2 μm) by ultrafiltration vacuum system. The precipitated or deposited particles are gold palladium coated and an ULTRA PLUS field emission scanning electron microscope (FE-SEM Carl Zeiss, Germany) is used to observe particles' morphology. Transmission electron microscope and Cryo-transmission electron microscope is also used to characterize the samples. It is worth highlighting that all nanoparticles are purified in ethanol to remove partially the unreacted reagents and to allow us the SEM characterization deposing the sample on a polycarbonate Isopore membrane filter (0.015, 0.05 and 0.1 μm) by ultrafiltration vacuum system.

### Loading capability

Loading capability is calculated collecting data by induced coupled plasma (ICP-MS), NexION® 350 Perkin Elmer Spectrometer. Nanoparticles are suspended in a solution of deionized water at a concentration of 250,000 particles/ml. Nanoparticles tracking analysis is used to calculate the number of nanoparticles (see Supplementary Figure 9). An acid compound is not added to avoid dissolution of the nanoparticles. All data are collected and processed using the Syngistix Nano Application Module. Gd is measured at m/z 157 using a 100 μs dwell time with no settling time.

The lyophilization of cHANPs is performed using a freeze-dryer Christ, 1–4LSC. Briefly, a freezing step for 3 h at -8°C with a cooling profile of 1°C/min is applied, sublimation at a shelf temperature of 6°C and pressure of 0.85 mbar for at least 24 h and finally, secondary drying at 25°C and 0.03 mbar for 5–6 h. Trehalose or sucrose ranging from 1 to 3% w/v is added

as cryoprotector if necessary for resuspension. Dried particles are also observed by FE-SEM.

### Stability & release study of cHANPs

The Gd-DTPA loaded cHANPs are mixed with 150 µl of PBS. The nanoparticles are kept shaking at 100 r.p.m. at 37°C. The solution is divided into two equal parts at 4, 12, 24, 48, 96 and 172 h post incubation. One-half of the solution is assessed by ICP-MS for the total concentration of $Gd^{3+}$ ions loaded within the nanoparticles. The other half of the solution is filter-spun using 0.45 µm filter columns at 14,000 r.p.m. for 5 min and the filtrate is analyzed for $Gd^{3+}$ ions. The two concentrations are compared and the amount of $Gd^{3+}$ ions released over time is determined. To assess the long stability of the nanoparticles, only conditions that do not produce a swelling behavior are tested. The release profile of Gd-DTPA is measured at different time points, namely 12, 24 and 48 h both in water and under two physiologically relevant conditions, namely stationary and constant shaking in PBS (pH = 7.4, 37°C).

### *In vitro* relaxivity study

Empty nanoparticles and nanoparticles containing Gd-DTPA at different concentrations are tested by *in vitro* MRI and results are compared with Magnevist, Gd-DTPA in water as a control. After vigorously stirring, changes in longitudinal relaxation time ($T_1$) are evaluated at 1.5 T by Minispec Bench Top Relaxometer (Bruker Corporation), adding 300 µl of the sample to a specific tube. Only results about $T_1$ will be reported. Finally, relaxivity $r_1$ is calculated using weighted linear regression ($R_1 = 1/T_1$ $s^{-1}$ relaxation rate plotted against Gd concentration, mM and $r_1$, $mM^{-1}$ $s^{-1}$, is the slope of the fitted curve). Estimation of measurement uncertainty is evaluated using weighted linear regression. Furthermore, the relaxation time distribution was obtained by CONTIN Algorithm. The relaxation spectrum was normalized with respect to the CONTIN processing parameters. The integral of a peak corresponds therefore to the contribution of the species exhibiting this peculiar relaxation to the relaxation time spectrum.

### Swelling ratio & hydrogel parameters

SR is calculated with Equation 1:

$$SR = \frac{d_{H2O}}{d_{eth}}$$

where $d_{eth}$ (in nm) $d_{H2O}$ (in nm) are the nanoparticle's diameters in ethanol and in water respectively (for further details about the SR calculation please refer to the Supplementary Information at the paragraph 'Calcula-

tions of the hydrogel network parameters'), measured by dynamic light scattering. A simplified version of the the Flory–Rehner equations are used in order to compute the hydrogel structure parameters ($\overline{Mc}$: Molecular weight between crosslinks (g/mol); $\nu_e$: Effective crosslink density (mol/cm³); $\xi$: Mesh size (nm)). See Supplementary Information for detailed calculations of the hydrogel network parameters.

## Results

### Preparation of cHANPs

MFF systems have already been explored for the production of polymer micelles and nanoparticles [48,49]. However, an investigation of the opportunity that this approach could bring to the MRI field, given the impact of the hydrogel behavior on the relaxometric properties, is still missing. We have recently demonstrated that, through the microfluidics, it is possible to produce stable hydrogel nanoparticles with improved relaxometric properties [35]. Briefly, by changing the relative flow rates and the concentration of the species in the streams, we can control nanoprecipitation phenomena [49–51] and achieve the formation of small nanoparticles (see Supplementary Table 1 & Figure 2). In our system, starting from an HA 0.05% w/v solution, monodisperse nanoparticles smaller than 40 nm are obtained (see Supplementary Figure 2B & C). Subsequently, a crosslinking reaction is performed together with the formation of nanoparticles using DVS [52–55] as crosslinking agent at standard flow conditions. In the same work [35], we have also reported two effective crosslinking scenarios to explore and control the nature of the interference (see Supplementary Figure 3 & Table 2) between the Gd-DTPA and the flow-focused nanoprecipitation: premixing of DVS into the middle channel at controlled temperature and surfactant concentration; addition of DVS to the side channels by strictly controlling pH conditions. Both strategies, exploited through the microfluidic platform, have been already reported [35] and further details in terms of crosslinking reaction and loading capability are reported in the Supplementary Figure 4 & Table 3. Results showing cHANPs with different concentration of NaOH and NaCl and different types of surfactants are already reported in our previous publication [35]. Briefly, spherical and stable nanoaprticles are obtained for both strategy but the addition of DVS to the middle channel and the use of surfactants produce a smaller size down to 35 nm.

### Swelling behavior & hydrogel structural parameters of cHANPs

Here, starting from results in terms of the SR, crosslink density and mesh size of the cHANPs containing Gd-DTPA are discussed, aiming to evaluate the
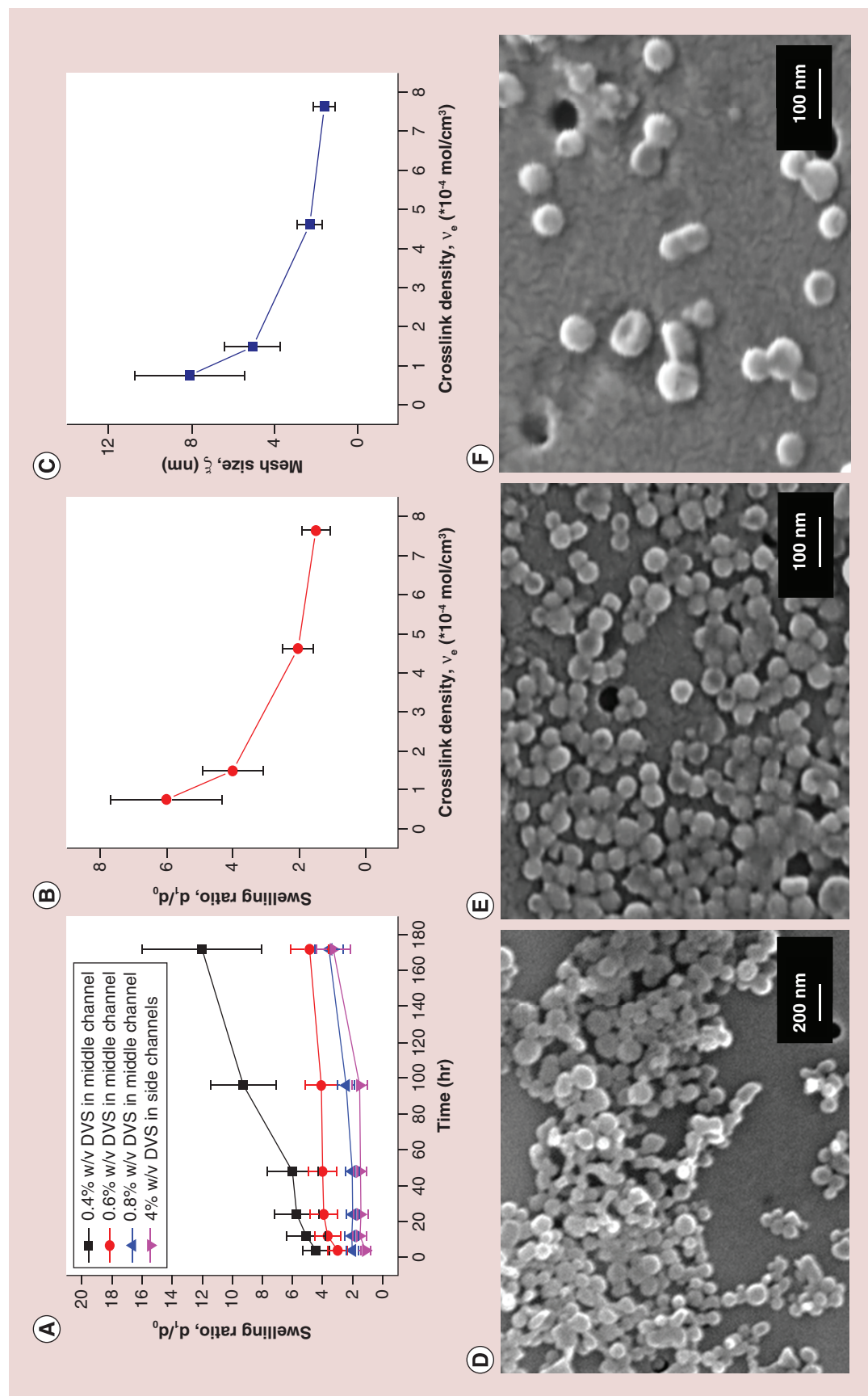
**Figure 1. Swelling behavior and hydrogel parameters of crosslinked hyaluronic acid nanoparticles. (A)** SR of of Gd-DTPA loaded cHANPs versus time at different DVS concentrations obtained according to the first (DVS in middle channel) or the second crosslinking scenario (DVS in side channels). **(B) & C)** SR (-•-) and mesh size (-■-) of Gd-DTPA loaded cHANPs versus crosslink density after 48 h in water. **(D & E)** FE-SEM images of Gd-DTPA loaded cHANPs in water at 0.8% DVS (middle channel) and 4% DVS (side channels), respectively. **(F)** 15° C tilted FE-SEM image of Gd-DTPA loaded cHANPs at 4%.
cHANP: Crosslinked hyaluronic acid nanoparticle; DVS: Divinyl sulfone; FE-SEM: Field emission scanning electron microscope; SR: Swelling ratio.
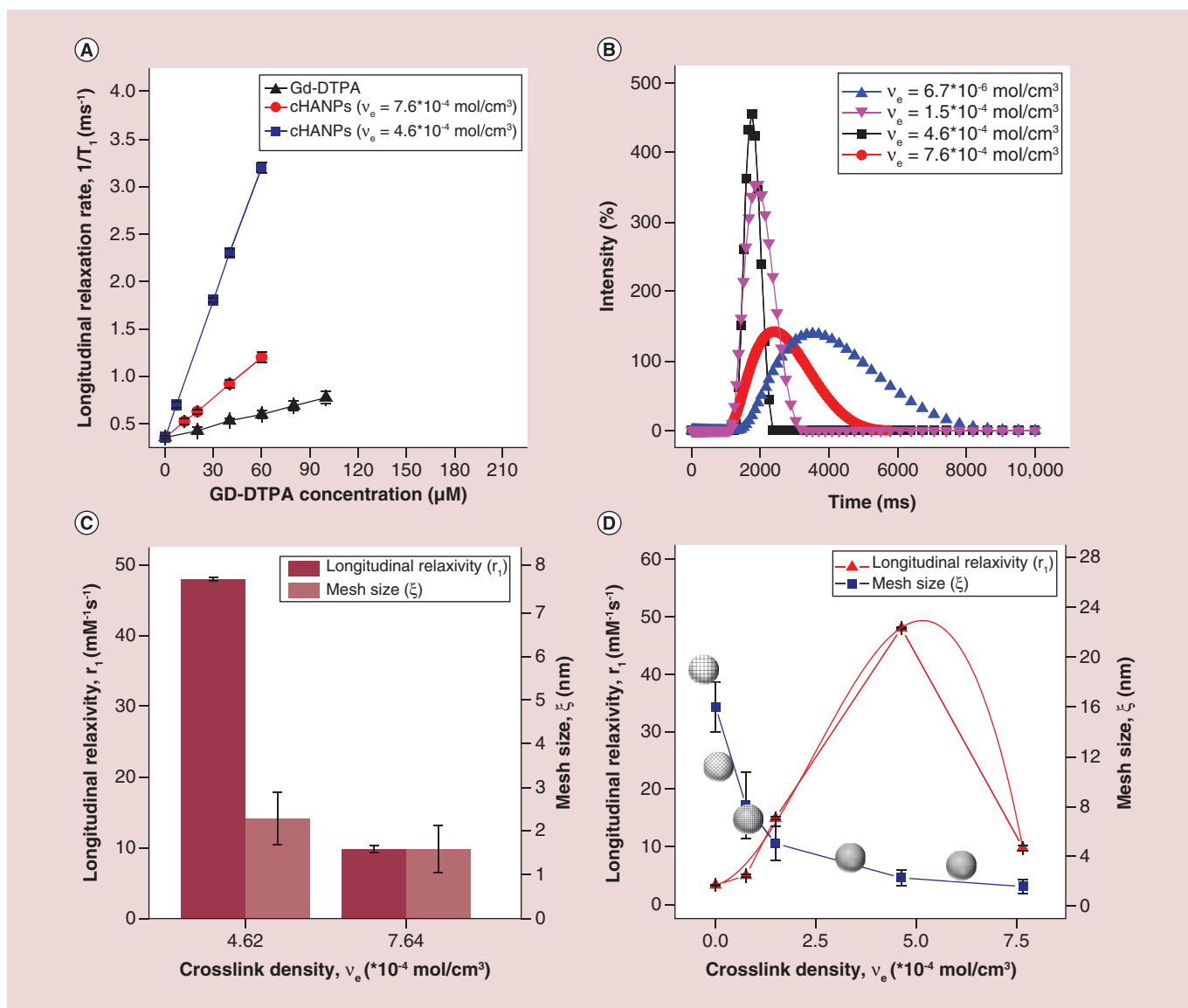
**Figure 2. *In vitro* magnetic resonance imaging and effect of the hydrodenticity. (A)** Longitudinal relaxation rate ($1/T_1$) versus Gd-DTPA concentration for (-▲-) free Gd-DTPA in water and for Gd-DTPA loaded cHANPs at different crosslink densities (-•- 7.6 × $10^{-4}$ and -■- 4.6 × $10^{-4}$ mol/cm³), showing a relaxivity of 3.9, 14.09 and 48.97 mM⁻¹s⁻¹, respectively. **(B)** Longitudinal relaxation time distribution for cHANPs at different crosslink densities. **(C)** Bar chart of longitudinal relaxivity (gray columns) and mesh size (blue columns) values for cHANPs at different crosslink densities. **(D)** Mesh size versus crosslink density (-•-) and corresponding relaxivity values (-▲-) along with a graphical representation of cHANPs' polymer network at different mesh size values.
cHANP: Crosslinked hyaluronic acid nanoparticle.

modulation of the hydrogel structure in the presence of Gd-DTPA.

As far as the swelling behavior of the nanoparticles, results at different DVS amounts are reported in Figure 1A and presented in terms of SR, as defined in the Methods section. Results clearly show that, nanoparticles are stable and do not exhibit a significant swelling behavior until 48 h at all explored DVS conditions (see also Supplementary Figures 5 & 6). In particular, smallest nanoparticles of about 70 and 50 nm

measured in water are only produced at DVS of 0.8 and 4% v/v, respectively. For these two conditions, an increase in size up to 125 nm for 0.8% DVS and 115 nm for 4% DVS is detected only after 1 week (see Supplementary Table 4).

Then, according to Flory–Rehner calculations [56], we have determined the crosslink density ($\nu_e$) and mesh size ($\xi$) of cHANPs in water after 48 h (see Supplementary Table 5). It has been already reported [53] that lower molecular weight films gave

rise to decreased molecular weights between crosslinks as well as increased effective crosslink densities and decreased mesh size, thereby indicating a more stable structure. Even our results show that a general increase of the crosslink density of the cHANPs corresponds to an increase in the nanostructure stability, in other words, lower swelling ratio (Figure 1B). Furthermore, as expected, by increasing the crosslink density, a reduction in mesh size is also obtained until to a certain extent (Figure 1C).

FE-SEM images of cHANPs at 0.8% DVS (middle channel) and 4% DVS (side channels) after 48 h in water are reported in Figure 1D, E & F. Higher DVS concentrations cause formation of large aggregates, as shown in Supplementary Figure 4A & B. It is important to highlight that cHANPS are potentially safe and biocompatible; indeed, even if DVS is highly reactive and toxic, HA-DVS biocompatibility has been confirmed by histological analysis, as previously reported by Oh *et al.* [57].

### *In vitro* relaxometric properties

The relationship between the measured structural parameters of the hydrogel and changes in CA's relaxivity is also examined (Figure 2).

Given the versatility of the produced cHANPs, it is of particular interest to investigate how different reaction's strategies and formulations could result in advanced and tailorable CA-loading functionalities. *In vitro* relaxivity is studied for loaded and unloaded cHANPs and the results are presented for Gd-DTPA in water at different concentrations. For all magnetic resonance (MR) experiments, $T_1$ values measured on loaded cHANPs show a higher relaxation rate compared with the relative 'free' CA, confirming that active compounds are not only dispersed or encapsulated but even wrapped within the hydrogel polymer matrix of cHANPs. Besides, it is observed that the hydrogel structural parameters, in other words, crosslink density and mesh size, can affect not only the stability and degradation behavior but also the MR functionality of the produced nanoparticles. Indeed, loaded cHANPs with different crosslink densities show a relaxivity ($r_1$) of about 48.97 and 14.09 mM$^{-1}$s$^{-1}$, respectively (Figure 2A, squares and circles). Both values are considerably higher than the value of 3.9 mM$^{-1}$s$^{-1}$ reported for commercial Magnevist (Figure 2A, triangles).

Additionally, a change in the crosslink densities of cHANPs causes differences in longitudinal relaxation time distributions (Figure 2B). A narrow distribution is obtained at a crosslink density of about 4.62 × 10$^{-4}$ mol/cm$^3$, reflecting optimal equilibrium conditions able to boost the MRI signal. Contrary to

expectations, further increase in the crosslink density does not allow a sharper relaxation time distribution, even at smaller mesh sizes. As shown in Figure 2C, in fact, even if the mesh sizes computed at two different crosslink densities are quite similar (1.5 and 2 nm for crosslink densities of 7.64 × 10$^{-4}$ and 4.62 × 10$^{-4}$ mol/cm$^3$, respectively), the highest relaxivity is not observed at the maximum crosslink density. This observation strenghtens the hypothesis that an optimal equilibrium among the species should be achieved in order to boost the relaxometric properties and that the hydrogel structure plays a critical role in the relaxation enhancement (see Figure 2D).

For completeness, we have also evaluated the relaxivity of unloaded cHANPs and cHANPs entrapping Gd-DTPA by sorption and compared with free Gd-DTPA in water (see Supplementary Figures 7 & 8).

The comparison of MRI relaxivity values acquired for cHANPs and free Gd-DTPA supports our initial hypothesis made on *Hydrodenticity*, revealing the opportunity to select specifically the optimal range of conditions that promotes relaxation enhancement (Figure 2D). Hence, the high relaxivity is attributed to the equilibrium simultaneously achieved between the water content within the hydrogel structures, expelled or retained during nanoprecipitation and crosslinking reaction, and the amount of Gd-DTPA entrapped in the formed matrix.

### Discussion

By the above reported experiments, we have proved that a systematic and accurate tunability can be achieved by varying the crosslinking degree of the hydrogel nanoparticles in the presence of Gd-DTPA. A narrow or a broad distribution of relaxation rates on the crosslink density is showed with regards to changes in the water dynamics, hydrogel conformation and slow motion of the CAs. High control of these parameters is mainly reached through a MFF approach [35].

Starting from the observation of a peculiar swelling behavior (Figure 1A) and *in vitro* relaxometric properties of the cHANPs (Figure 2), we propose an explanation, through a modified Flory–Rheiner theory, of how the hydrogel structural parameters can be used to improve the relaxometric properties of CAs [53].

Results show that *Hydrodenticity* can be proposed as a new concept to summarize the complex equilibrium formed by elastic stretches of polymer chains, water osmotic pressure and hydration degree of GdCAs able to boost the relaxivity.

Indeed, at the achieved minimum mesh size, crosslink density is responsible for the elastodynamic of the hydrogel and is representative of the water amount within the polymer meshes, which in turn is related
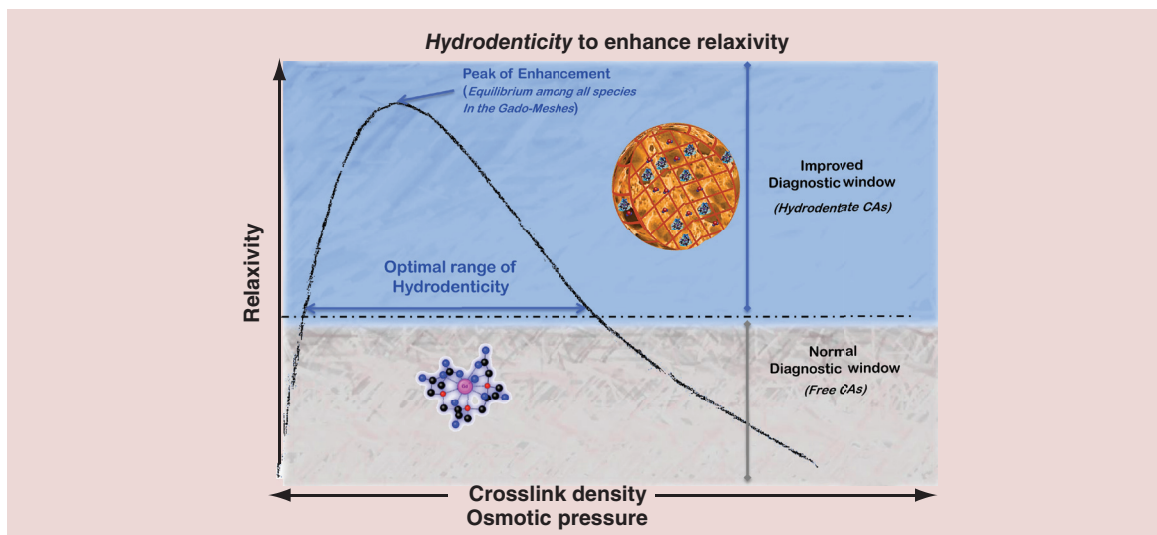
**Figure 3. *Hydrodenticity* to enhance relaxivity.** Schematic illustration of an improved diagnostic window in which it is possible to obtain a medical device for clinical use in the MRI field able to overcome the limitations related to the use of commercial CAs such as low relaxivity, limited acquisition time and reduced tissue specificity.
CA: Contrast agent; MRI: Magnetic resonance imaging.

to the osmotic pressure. Our results also show that the reduction in the elasticity of the matrix by increasing the crosslink density does not correspond to a maximum enhancement of the relaxivity (see Figure 2D). It is probably due to the expelled water from the hydrogel network [54] that causes a reduction in the osmotic pressure within the water compartments of the meshes and a decrease of the hydrated status of Gd-DTPA, thus limiting the enhancement of the relaxometric properties in the nanostructures. These conditions promote the formation of water compartments containing Gd-DTPA called 'Gado-Meshes'.

It is also well-known that the crosslink density acts on the water diffusion, which decreases when the crosslink density increases and its slowdown in diffusion is more severe at the polymer–water interface [58,59]. Even in the Gd-loaded cHANPs, the water diffusion at various crosslink densities is correlated with the water hydrogen bonding dynamics and the variation of diffusion coefficient with crosslink density is related to the variation of water content in different crosslink densities. Therefore, by changing further the properties of the 'Gado-Meshes' through the crosslinking reaction, relaxivity increases to an even greater extent due to the *Hydrodenticity* because of the tuning of the crosslink density and, consequently, of the aggregated water state and slow moving of the CAs.

As the *Hydrodenticity* of CAs within the Gado-Mesh does not involve the chemical modification of the CAs, the observed enhancement in relaxivity is induced by the synergistic interaction of the aggregated water with the hydrogel matrix and Gd-DTPA. Indeed, according to the Solomon–Bloembergen–Morgan theory, this effect promotes both (§) a further reduction of the water mobility and diffusion, inducing an increase of the residence lifetime and characteristic diffusion time ($T_D$) of inner and outer sphere water molecules; and (§§) changes in hydrogel structures leading to the formation of nanocompartments enwrapping GdCAs, causing a slow motion of the CAs and, therefore, an increase of the rotational correlation time of the chelate. Furthermore, it is reasonable that the conditions reached in the Gado-Mesh can control the water exchange and therefore, the relaxivity. Indeed, relaxivity can be limited if the water exchange is too slow because the relaxation effect is poorly transmitted to the bulk. However, relaxivity can also be reduced if the water exchange is too fast because the water is not coordinated to the GdCAs long enough to be relaxed [60].

In the proposed system, at some degree of *Hydrodenticity*, the hydrated status of Gd complexes, the elastodynamic response of HA and the osmotic pressure results probably in a much slower rotation. At this point, the importance of water exchange becomes significant, but the improved relaxivity of Gd-loaded cHANPs confirms that water diffusion is high enough and the process for relaxing the water protons of aggregated water is in any case very efficient. Finally, the relaxation time measurements clearly demonstrate how cHANPs themselves do not contribute to the relaxivity of the system (see Supplementary Figure 8). Thus, the increase in the relaxivity of the loaded cHANPs can be attributed solely to the formation of the Gado-Mesh and to the *Hydrodenticity* achieved in their organization that influences the relaxivity

through the characteristic correlation times above mentioned.

Modulation of the *Hydrodenticity* through the elastic stretching of the polymer meshes, osmotic pressure and hydrated state of Gd-DTPA contributes to the changes of the inner and outer sphere mechanisms of the CAs. Therefore, through the hydrogel structural parameters, we can produce a library of functional nanostructures on the needs of a particular pathology, field and material properties. Results could lead to the identification of a personalized diagnostic window (Figure 3) that can define the range of optimal properties between the hydrogel matrix and the CAs, being more efficient in treating a particular disease, avoiding toxic effects and increasing the performance of the MRI acquisitions.

## Conclusion

The introduction of the *Hydrodenticity* creates significant opportunities in controlling the behavior of metal chelates without their chemical modifications. It enables the increase of the relaxometric properties of the CAs preserving the chemical structures as approved for the use in the clinical practice. The possibility to increase the sensitivity of the CAs represents an opportunity to reduce the administration dosage currently in use.

Furthermore, Gd-loaded cHANPs based on the concept of *Hydrodenticity* are candidate to become

an important nanomedicine tool to be tested in this direction, exhibiting a relaxivity value of ~48.9 and ~14.02 mM$^{-1}$s$^{-1}$. Additionally, cHANPs have an average diameter of about 35 nm, do not swell nor degrade for at least 48 h under shaking. Further benefits can be found in: the possibility to be decorated chemically, becoming suitable for a specific target; the direct clinical application, due to the utilization and improvement of biocompatible and US FDA approved products without their chemical modifications; the ease of the synthesis; the nature of the materials; and the scalability of the proposed process. In the future, the concept of *Hydrodenticity* could inspire other applications and be extended to different molecules and field of knowledge.

---

### Summary points

- Clinically used contrast agents (CAs) for magnetic resonance imaging still suffer from poor sensitivity, low relaxivity and risk of metal ion deposition.
- We showed how hydrogel materials could respond to the dual need of protecting those CAs from transmetallation and at the same time, significantly improve their efficacy.
- We adopted a microfluidic flow focusing approach to produce crosslinked hyaluronic acid nanoparticles (cHANPs) that encapsulate gadolinium (Gd)-DTPA without chemically modifying its structure and biocompatibility.
- Swelling and relaxometric properties of the cHANPs were measured and studied using different techniques, from scanning electron microscopy and dynamic light scattering to time-domain nuclear magnetic resonance relaxometry.
- Hydrogel parameters of the cHANPs, in other words, mesh size and crosslink density, were computed using Flory–Rehner equations and related to the relaxometric properties of the produced nanostructures.
- We pointed out and theoretically demonstrated that Gd-DTPA relaxometric properties can be modulated by tuning the hydrogel structure of cHANPs through a microfluidic platform.
- The complex equilibrium established by the elastic stretches of polymer chains, water osmotic pressure and hydration degree of Gd-DTPA, able to boost the relaxometric properties of Gd-DTPA, is here defined and called *Hydrodenticity*.
- The new concept is used to explain the increase (12-times) in Gd-DTPA relaxivity, achieved through the production of 35 nm cHANPs.
- Within the cHANPs, the properties of *Hydrodenticity* can be modulated to obtain desired crosslink density, mesh size, hydrophilicity and loading capability, playing on the biodegradable behavior and relaxometric properties of the Gd-loaded cHANPs.
- The capability to control this equilibrium within the nanoparticles can be applied to define a new class of medical devices useful to improve the properties of magnetic resonance imaging CAs.

## References

1    Holbrook RJ, Rammohan N, Rotz MW, Macrenaris KW, Preslar AT, Meade TJ. Gd(III)-dithiolane gold nanoparticles for T-1-weighted magnetic resonance imaging of the pancreas. *Nano Lett.* 16(5), 3202–3209 (2016).

2    Chang Y, Lee GH, Kim T-J, Chae K-S. Toxicity of magnetic resonance imaging agents: small molecule and nanoparticle. *Curr. Top. Med. Chem.* 13(4), 434–445 (2013).

3    Ni Y. MR contrast agents for cardiac imaging. In: *Clinical Cardiac MRI.* Springer, 31–51 (2011).

4    Arosio P, Thevenot J, Orlando T *et al.* Hybrid iron oxide-copolymer micelles and vesicles as contrast agents for MRI: impact of the nanostructure on the relaxometric properties. *J. Mater. Chem. B* 1(39), 5317–5328 (2013).

5    Xue S, Qiao J, Pu F, Cameron M, Yang JJ. Design of a novel class of protein-based magnetic resonance imaging contrast agents for the molecular imaging of cancer biomarkers. *Wiley Interdiscip. Rev. Nanomed. Nanobiotechnol.* 5(2), 163–179 (2013).

6    Lee N, Yoo D, Ling D, Cho MH, Hyeon T, Cheon J. Iron oxide based nanoparticles for multimodal imaging and magnetoresponsive therapy. *Chem. Rev.* 115(19), 10637–10689 (2015).

7    Iagaru A, Mittra E, Minamimoto R *et al.* Simultaneous whole-body time-of-flight F-18-FDG PET/MRI A pilot study comparing SUVmax with PET/CT and assessment of MR image quality. *Clin. Nucl. Med.* 40(1), 1–8 (2015).

8    Sampath SC, Mosci C, Lutz AM *et al.* Detection of osseous metastasis by F-18-NaF/F-18-FDG PET/CT versus CT alone. *Clin. Nucl. Med.* 40(3), E173–E177 (2015).

9    Do C, Barnes JL, Tan C, Wagner B. Type of MRI contrast, tissue gadolinium, and fibrosis. *Am. J. Physiol. Renal Physiol.* 307(7), F844–F855 (2014).

10   Guglielmo FF, Mitchell DG, Gupta S. Gadolinium contrast agent selection and optimal use for body MR imaging. *Radiol. Clin. North Am.* 52(4), 637–+ (2014).

11   Garcia J, Tang T, Louie AY. Nanoparticle-based multimodal PET/MRI probes. *Nanomedicine* 10(8), 1343–1359 (2015).

12   Wang Y-XJ. Superparamagnetic iron oxide based MRI contrast agents: current status of clinical application. *Quant. Imaging Med. Surg.* 1(1), 35–40 (2011).

13   Weidman EK, Dean KE, Rivera W, Loftus ML, Stokes TW, Min RJ. MRI safety: a report of current practice and advancements in patient preparation and screening. *Clin. Imaging* 39(6), 935–937 (2015).

14   Caravan P. Strategies for increasing the sensitivity of gadolinium based MRI contrast agents. *Chem. Soc. Rev.* 35(6), 512–523 (2006).

15   Shetty AN, Pautler R, Ghagahda K *et al.* A liposomal Gd contrast agent does not cross the mouse placental barrier. *Sci. Rep.* 6, 27863 (2016).

16   Mcdonald RJ, Mcdonald JS, Kallmes DF *et al.* Intracranial gadolinium deposition after contrast-enhanced MR imaging. *Radiology* 275(3), 772–782 (2015).

17   Lux F, Sancey L, Bianchi A, Cremillieux Y, Roux S, Tillement O. Gadolinium-based nanoparticles for theranostic MRI-radiosensitization. *Nanomedicine* 10(11), 1801–1815 (2015).

18   Hou SJ, Tong S, Zhou J, Bao G. Block copolymer-based gadolinium nanoparticles as MRI contrast agents with high T-1 relaxivity. *Nanomedicine* 7(2), 211–218 (2012).

19   Frangville C, Li Y, Billotey C *et al.* Assembly of double-hydrophilic block copolymers triggered by gadolinium ions: new colloidal MRI contrast agents. *Nano Lett.* 16(7), 4069–4073 (2016).

20   Lesniak WG, Oskolkov N, Song X *et al.* Salicylic acid conjugated dendrimers are a tunable, high performance CEST MRI nanoplatform. *Nano Lett.* 16(4), 2248–2253 (2016).

21   Hachani R, Lowdell M, Birchall M *et al.* Polyol synthesis, functionalisation, and biocompatibility studies of superparamagnetic iron oxide nanoparticles as potential MRI contrast agents. *Nanoscale* 8(6), 3278–3287 (2016).

22   Ni KY, Zhao ZH, Zhang ZJ *et al.* Geometrically confined ultrasmall gadolinium oxide nanoparticles boost the T-1 contrast ability. *Nanoscale* 8(6), 3768–3774 (2016).

23   Zhang L, Liu RQ, Peng H, Li PH, Xu ZS, Whittaker AK. The evolution of gadolinium based contrast agents: from single-modality to multi-modality. *Nanoscale* 8(20), 10491–10510 (2016).

24   Opina AC, Wong KJ, Griffiths GL *et al.* Preparation and long-term biodistribution studies of a PAMAM dendrimer G5-Gd-BnDOTA conjugate for lymphatic imaging. *Nanomedicine* 10(9), 1423–1437 (2015).

25   Solomon I. Relaxation processes in a system of two spins. *Phys. Rev.* 99(2), 559 (1955).

26   Bloembergen N. Proton relaxation times in paramagnetic solutions. *J. Chem. Phys.* 27(2), 572–573 (1957).

27   Rotz MW, Culver KSB, Parigi G *et al.* High relaxivity Gd(III) – DNA gold nanostars: investigation of shape effects on proton relaxation. *ACS Nano* 9(3), 3385–3396 (2015).

28   Wang ZT, Zhao LJ, Yang P, Lv ZW, Sun H, Jiang Q. Water-soluble amorphous iron oxide nanoparticles synthesized by a quickly pestling and nontoxic method at room temperature as MRI contrast agents. *Chem. Eng. J.* 235, 231–235 (2014).

29   Wang GS, Ma YY, Wei ZY, Qi M. Development of multifunctional cobalt ferrite/graphene oxide nanocomposites for magnetic resonance imaging and controlled drug delivery. *Chem. Eng. J.* 289, 150–160 (2016).

30   Lakshmanan S, Holmes WM, Sloan WT, Phoenix VR. Nanoparticle transport in saturated porous medium using magnetic resonance imaging. *Chem. Eng. J.* 266, 156–162 (2015).

31   Skotland T, Iversen TG, Sandvig K. Development of nano-particles for clinical use. *Nanomedicine* 9(9), 1295–1299 (2014).

32   Butterworth KT, Nicol JR, Ghita M *et al.* Preclinical evaluation of gold-DTDTPA nanoparticles as theranostic agents in prostate cancer radiotherapy. *Nanomedicine* 11(16), 2035–2047 (2016).

33   Vecchione D, Grimaldi A, Forte E, Bevilacqua P, Netti P, Torino E. Hybrid Core-Shell (HyCoS) nanoparticles produced by complex coacervation for multimodal applications. *Sci. Rep.* 7, 45121 (2017).

34  Ponsiglione AM, Russo M, Netti PA, Torino E. Impact of biopolymer matrices on relaxometric properties of contrast agents. *Interface Focus* 6(6), 20160061–20160061 (2016).

35  Russo M, Bevilacqua P, Netti PA, Torino E. A microfluidic platform to design crosslinked hyaluronic acid nanoparticles (cHANPs) for enhanced MRI. *Sci. Rep.* 6, 37906 (2016).

36  Port M, Raynal I, Elst LV *et al.* Impact of rigidification on relaxometric properties of a tricyclic tetraazatriacetic gadolinium chelate. *Contrast Media Mol. Imaging* 1(3), 121–127 (2006).

37  Sethi R, Ananta JS, Karmonik C *et al.* Enhanced MRI relaxivity of Gd3+-based contrast agents geometrically confined within porous nanoconstructs. *Contrast Media Mol. Imaging* 7(6), 501–508 (2012).

38  Courant T, Roullin VG, Cadiou C *et al.* Hydrogels incorporating GdDOTA: towards highly efficient dual T1/T2 MRI contrast agents. *Angew. Chem. Int. Edit.* 51(36), 9119–9122 (2012).

39  Bryson JM, Reineke JW, Reineke TM. Macromolecular imaging agents containing lanthanides: can conceptual promise lead to clinical potential? *Macromolecules* 45(22), 8939–8952 (2012).

40  Kircher MF, De La Zerda A, Jokerst JV *et al.* A brain tumor molecular imaging strategy using a new triple-modality MRI-photoacoustic-Raman nanoparticle. *Nat. Med.* 18(5), U829–U235 (2012).

41  Cole AJ, David AE, Wang J, Galban CJ, Yang VC. Magnetic brain tumor targeting and biodistribution of long-circulating PEG-modified, cross-linked starch-coated iron oxide nanoparticles. *Biomaterials* 32(26), 6291–6301 (2011).

42  Kabiri M, Unsworth LD. Application of isothermal titration calorimetry for characterizing thermodynamic parameters of biomolecular interactions: peptide self-assembly and protein adsorption case studies. *Biomacromolecules* 15(10), 3463–3473 (2014).

43  Velasco D, Tumarkin E, Kumacheva E. Microfluidic encapsulation of cells in polymer microgels. *Small* 8(11), 1633–1642 (2012).

44  Khabaz F, Mani S, Khare R. Molecular origins of dynamic coupling between water and hydrated polyacrylate gels. *Macromolecules* 49(19), 7551–7562 (2016).

45  Strom A, Larsson A, Okay O. Preparation and physical properties of hyaluronic acid-based cryogels. *J. Appl. Polym. Sci.* 132(29), 42194 (2015).

46  Utech S, Boccaccini AR. A review of hydrogel-based composites for biomedical applications: enhancement of hydrogel properties by addition of rigid inorganic fillers. *J. Mater. Sci.* 51(1), 271–310 (2016).

47  Bicudo RCS, Santana MHA. Production of hyaluronic acid (HA) nanoparticles by a continuous process inside microchannels: effects of non-solvents, organic phase flow rate, and HA concentration. *Chem. Eng. Sci.* 84, 134–141 (2012).

48  Souza Bicudo RC, Andrade Santana MH. Production of hyaluronic acid (HA) nanoparticles by a continuous process inside microchannels: effects of non-solvents, organic phase flow rate, and HA concentration. *Chem. Eng. Sci.* 84, 134–141 (2012).

49  Capretto L, Cheng W, Carugo D, Katsamenis OL, Hill M, Zhang XL. Mechanism of co-nanoprecipitation of organic actives and block copolymers in a microfluidic environment. *Nanotechnology* 23(37), 16 (2012).

50  Anton N, Bally F, Serra CA *et al.* A new microfluidic setup for precise control of the polymer nanoprecipitation process and lipophilic drug encapsulation. *Soft Matter* 8(41), 10628–10635 (2012).

51  Sah E, Sah H. Recent trends in preparation of poly(lactide-co-glycolide) nanoparticles by mixing polymeric organic solution with antisolvent. *J. Nanomater.* 2015, 794601 (2015).

52  Collins MN, Birkinshaw C. Comparison of the effectiveness of four different crosslinking agents with hyaluronic acid hydrogel films for tisslue-culture applications. *J. Appl. Polym. Sci.* 104(5), 3183–3191 (2007).

53  Collins MN, Birkinshaw C. Investigation of the swelling behavior of crosslinked hyaluronic acid films and hydrogels produced using homogeneous reactions. *J. Appl. Polym. Sci.* 109(2), 923–931 (2008).

54  Martins Shimojo AA, Barbosa Pires AM, Lichy R, Rodrigues AA, Andrade Santana MH. The crosslinking degree controls the mechanical, rheological, and swelling properties of hyaluronic acid microparticles. *J. Biomed. Mater. Res. A* 103(2), 730–737 (2015).

55  Shimojo AaM, Pires AMB, Lichy R, Santana MHA. The performance of crosslinking with divinyl sulfone as controlled by the interplay between the chemical modification and conformation of hyaluronic acid. *J. Braz. Chem. Soc.* 26(3), 506–512 (2015).

56  Leach JB, Bivens KA, Patrick CW, Schmidt CE. Photocrosslinked hyaluronic acid hydrogels: natural, biodegradable tissue engineering scaffolds. *Biotechnol. Bioeng.* 82(5), 578–589 (2003).

57  Oh EJ, Kang S-W, Kim B-S, Jiang G, Cho IH, Hahn SK. Control of the molecular degradation of hyaluronic acid hydrogels for tissue augmentation. *J. Biomed. Mater. Res. A* 86A(3), 685–693 (2008).

58  Wu Y, Joseph S, Aluru NR. Effect of cross-linking on the diffusion of water, ions, and small molecules in hydrogels. *J. Phys. Chem. B* 113(11), 3512–3520 (2009).

59  Ori G, Massobrio C, Pradel A, Ribes M, Coasne B. Structure and dynamics of ionic liquids confined in amorphous porous chalcogenides. *Langmuir* 31(24), 6742–6751 (2015).

60  Demello J, Demello A. Microscale reactors: nanoscale products. *Lab Chip* 4(2), N11–N15 (2004).